Wind Energ. Sci. Discuss., https://doi.org/10.5194/wes-2017-42
Manuscript under review for journal Wind Energ. Sci.
Discussion started: 9 October 2017

eawe european academy of wind energy
Open Access WIND ENERGY SCIENCE DISCUSSIONS

About the suitability of different numerical methods to reproduce model wind turbine measurements in a wind tunnel with high blockage ratio

Annette Claudia Klein[1], Sirko Bartholomay[2], David Marten[2], Thorsten Lutz[1], George Pechlivanoglou[2], Christian Navid Nayeri[2], Christian Oliver Paschereit[2], and Ewald Krämer[1]

[1]University of Stuttgart, Institute of Aerodynamics and Gas Dynamics, Pfaffenwaldring 21, 70569 Stuttgart, Germany
[2]TU Berlin, Chair of Fluid Dynamics, Müller-Breslau-Straße 8,10623 Berlin, Germany

Correspondence to: Annette Claudia Klein (annette.klein@iag.uni-stuttgart.de)

Abstract. Numerical and experimental investigations of a model wind turbine with a diameter of $3.0\mathrm{m}$ are described in the present paper. The objectives of the study are the provision of validation data, the comparison and evaluation of methods of different fidelity and the assessment of the influence of the wind tunnel walls by comparison of measurements to simulations with and without wind tunnel walls. The experiments were carried out in the large wind tunnel of the TU Berlin. With the Lifting Line Free Vortex Wake (*LLFVW*) code *QBlade*, the turbine was simulated under far field conditions at the TU Berlin. *URANS* simulations were performed at the University of Stuttgart with the *CFD* code *FLOWer* for far field condition to draw a comparison to *QBlade*. Moreover, *CFD* simulations of the turbine in a wind tunnel were carried out, as the walls have a significant influence on the turbine performance.

Comparisons between experiment, the *LLFVW* code and *CFD* include on-blade velocities, angle of attack and bending moments. Comparisons of flow fields are drawn between experiment and the *CFD* code.

A good accordance was achieved for the flow fields, the on-blade velocity and the angle of attack, whereas deviations occur for the bending moments.

1 Introduction

Although there was a huge advancement of wind turbine rotors over the last couple of years, the development and improvement do not come to a halt. New strategies and concepts are developed and have to be completely understood, before they can be applied on real wind turbines. In many cases, investigations take place on a model wind turbine, which is less expensive than building a full size prototype, and in a wind tunnel, where reproducible inflow conditions can be created. Simulations of a model wind turbine, as done in the *MEXICO* project (Schepers and Snel, 2007), can validate numerical methods and can lead to improvements of design methods. Blind tests, for example of unsteady aerodynamics experiment as done in the NASA-Ames wind tunnel (Simms et al., 2001), can be used to improve the development of wind turbine aerodynamics codes and the provided data can also be used for their validation.

Moreover, simulations of model wind turbines can extend the test matrix and therefore the knowledge about the behaviour of

Wind Energ. Sci. Discuss., https://doi.org/10.5194/wes-2017-42
Manuscript under review for journal Wind Energ. Sci.
Discussion started: 9 October 2017

the turbine and they can build the bridge to full size turbines. Depending on the computational capacity and the available time, low or high fidelity approaches can be used.

The model wind turbine *BeRT* (Berlin Research Turbine) (Pechlivanoglou et al., 2015), which is investigated in the present paper, was designed and built by TU Berlin and *SMART BLADE GmbH* with a contribution of TU Darmstadt in the aerodynamic blade design. The turbine was simulated with two methods with different degrees of complexity. Afterwards, the results were compared to the experimental results.

A Lifting Line Free Vortex Wake code (*QBlade*) simulates the turbine under free stream condition. In the numerical setup of the CFD code *FLOWer*, the wind tunnel walls and the nozzle are taken into account, but also a case with far field is simulated in order to get a better comparison to the *QBlade* results. The numerical and experimental investigation of the turbine is part of the *DFG PAK 780* project (Nayeri et al., 2015), where six partners from five universities work together in the field of wind turbine load control. Huang et al. (2015) already investigated a one third model of the turbine under uniform inflow in a far field environment with a large eddy simulation approach (*LES*) and Fischer et al. (2016) performed unsteady Reynolds-averaged Navier-Stokes-Equations (*URANS*) under uniform inflow in a far field environment, as well as in an approximated wind tunnel to estimate the influence of the blockage effect. Moreover, the influence of wind tunnel walls, tower and nozzle on the performance of a full model of the turbine was numerically investigated by Klein et al. (2017).

Three different states of the turbine are investigated in this paper. In all cases, uniform inflow is considered. In the baseline case (hereinafter called as $CaseBASE$), the turbine has $0°$ yaw misalignment. In $CaseYAW15$, the turbine is yawed by $-15°$ and in $CaseYAW30$ by $-30°$, respectively.

As loads on a turbine are a result of the flow around the rotor, in the present paper, the flow fields upstream and downstream of the turbine are analyzed. The on-blade velocities and angles of attack (AoA), as seen by defined blade sections, are compared between experiment, *QBlade* and *FLOWer*. As the determination of the AoA is very complex, in *CFD* two different methods are used. Moreover, the bending moments at the blade root are compared between experiment, *QBlade* and *FLOWer*.

The aims of the present study are the provision of experimental data for validation of the numerical approaches, the comparison of codes with different grades of fidelity and the evaluation of their suitability to simulate the model wind turbine and the influence of the wind tunnel walls.

2 Methodology and setups

2.1 Experimental setup

2.1.1 Wind tunnel

The experiments are carried out in the large wind tunnel (*GroWiKa*) of the TU Berlin, Fig. 1 (Bartholomay et al., 2017). Driven by a $450\mathrm{kW}$ fan, the test-section velocity reaches up to $60\mathrm{m/s}$. In the settling chamber ($4.2 \times 4.2\mathrm{m}^2$), where the turbine was

Wind Energ. Sci. Discuss., https://doi.org/10.5194/wes-2017-42
Manuscript under review for journal Wind Energ. Sci.
Discussion started: 9 October 2017

placed due to its large diameter, the maximum velocity is $10\mathrm{m/s}$ and the turbulence intensity is $Ti \leq 1.5\%$.

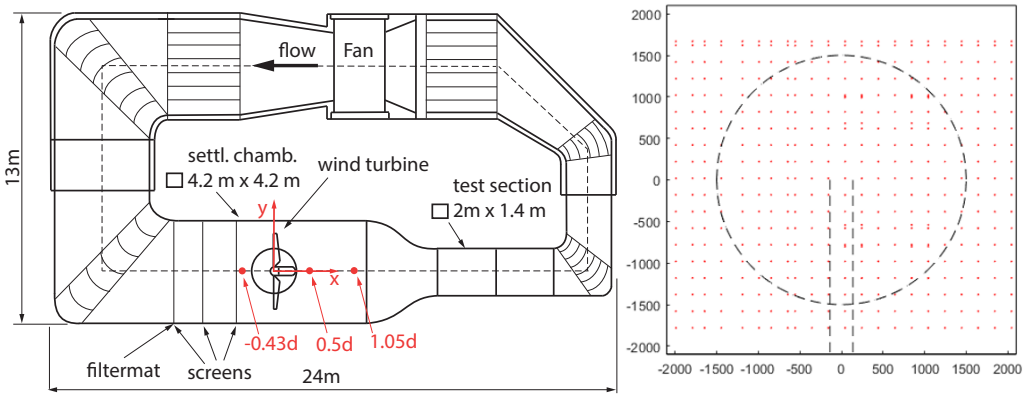

Figure 1. Large wind tunnel of the TU Berlin (left) and hot-wire measurement position in each cross-plane (right), (Bartholomay et al., 2017).

2.1.2 Berlin Research Turbine (*BeRT*)

The Berlin Research Turbine (*BeRT*), Fig. 2, has a rotor diameter of $3\mathrm{m}$ with a tower height of $2.1\mathrm{m}$. The three blades are exchangeable and equipped with a *Clark-Y* airfoil throughout the complete blade radius from tip to hub. This airfoil was used as is provides attached flow for low Reynolds numbers and a good effectiveness of flaps, which will be investigated on the turbine in future experiments and simulations. The twist was chosen so that the local angle of attack stays constant over the span. In order to get a defined transition position for the *CFD* simulations, zig-zag tape has been placed on the blades. The height of the turbulator is adapted to the boundary layer thickness, which varies with the rotor radius, and is consequently staggered. It amounts h=$0.75\mathrm{mm}$ inboard up to h=$0.21\mathrm{mm}$ outboard on the suction side and h=$0.95\mathrm{mm}$ inboard up to h=$0.50\mathrm{mm}$ outboard on the pressure side. On the suction side, the leading edge of the tape was positioned at 5% chord, on the pressure side at 10% chord.

The turbine data is summarized in Table 1 (Bartholomay et al., 2017; Pechlivanoglou et al., 2015; Vey et al., 2015).

The model creates a significant level of blockage of $\beta = A_{BeRT}/A_{tunnel} = 40\%$. This value is far beyond blockage ratios where correction methods have proven their applicability. However, the aim of this ongoing project is rather to analyze the relative impact and effectiveness of flow control devices and not to quantify the overall performance to a turbine in the far field. Data acquisition is achieved by *National Instrument* hardware in the rotating and in the non-rotating system. In the former, a *cRIO* platform rotates with the turbine and acquires data from sensors placed on the blades. In the non-rotating setup, a *National Instruments cDAQ* platform collects data from additional sensors, such as tower / nacelle acceleration and tower base strain for thrust measurements. Data transmission between the two systems and the control computer is achieved by *WiFi* connection.

Wind Energ. Sci. Discuss., https://doi.org/10.5194/wes-2017-42
Manuscript under review for journal Wind Energ. Sci.
Discussion started: 9 October 2017

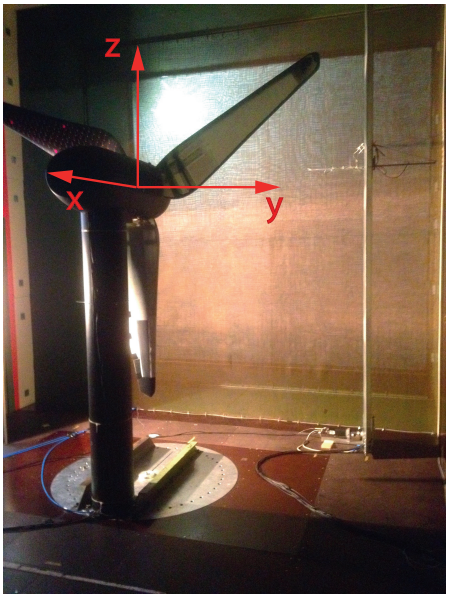

Figure 2. BeRT and hot-wire traversing system.

Table 1. Summary of the turbine specifics.

Tower height	2.1m
Tower diameter	0.273m
Rotor diameter	3.0m
Rotor overhang	0.5m
Rotor blade airfoil	Clark-Y
Rated RPM	$180 min^{-1}$
Inflow velocity	6.5m/s
TSR	4.35
3-hole probe position	$65\%R$, $75\%R$, $85\%R$

Further information on the setup is found in (Vey et al., 2015).

Wind Energ. Sci. Discuss., https://doi.org/10.5194/wes-2017-42
Manuscript under review for journal Wind Energ. Sci.
Discussion started: 9 October 2017

eawe european academy of wind energy
Open Access WIND ENERGY SCIENCE DISCUSSIONS

2.1.3 *BASELINE* and *SMART* blade

The turbine is equipped with two baseline blades and one smart blade. The smart blade is equipped with a multitude of sensors and actuators for trailing edge deployment, whereas one of the baseline blades is equipped with blade root bending sensors. Besides that, no other sensors or actuators are mounted on the baseline blades (Bartholomay et al., 2017).

The smart blade, Fig. 3, is equipped with pressure ports, strain gauges at the blade root, acceleration sensors at the tip, 3-hole probes to measure the angle of attack at $65\%R$, $75\%R$ and $85\%R$, trailing edge flap actuators and encoders to measure the flap position. For the current study, the flaps were not deflected but fixed in their neutral position (Bartholomay et al., 2017).

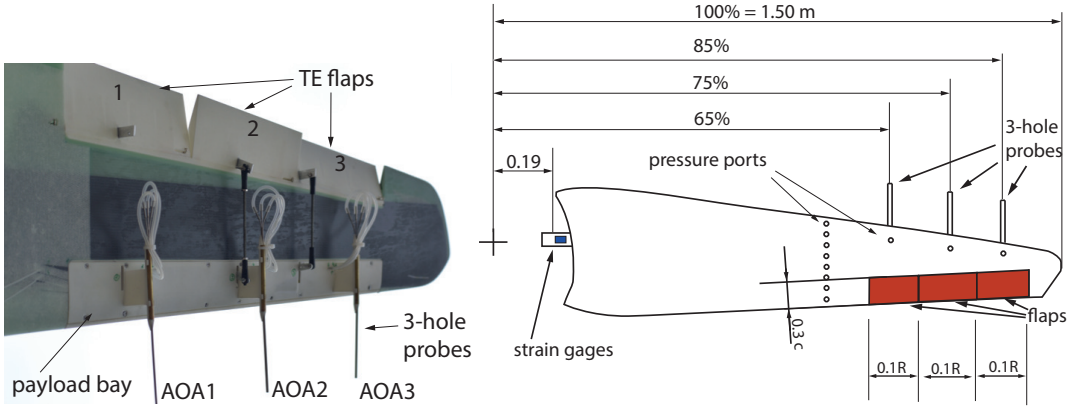

Figure 3. Smart blade, (Bartholomay et al., 2017).

2.2 The Lifting Line Free Vortex Wake Code *QBlade*

2.2.1 Numerical methods of *QBlade*

The Lifting Line Free Vortex Wake (*LLFVW*) computations in this study are performed with the wind turbine design and simulation tool *QBlade* (Marten et al., 2010, 2016, 2015), which has been developed and is still under development at the Technical University of Berlin. The *LLFVW* algorithm is loosely based on the non-linear lifting line formulation as described by Van Garrel (2003) and its implementation in *QBlade* is used to simulate both, HAWT and VAWT rotors.

Rotor forces are evaluated on a blade element basis from tabulated lift and drag polar data. The near and far wake is modelled with vortex line elements, which are shed at the blades trailing edge during every time step and then undergo free convection behind the rotor. Vortex elements are de-singularized using a cut off method (as described by Marten et al. (2016)) based on the vortex core size. Viscous diffusion in the wake is accounted for through vortex core growths term.

The tower shadow is taken into account by using a model derived from the work of Bak et al. (2001), in which the tower is modelled through a combination of the analytical potential flow around a cylinder superimposed with an empirical downwind wake model based on a tower drag coefficient.

Wind Energ. Sci. Discuss., https://doi.org/10.5194/wes-2017-42
Manuscript under review for journal Wind Energ. Sci.
Discussion started: 9 October 2017

The effects of unsteady aerodynamics and dynamic stall are introduced via the *ATEFlap* aerodynamic model (Wendler et al., 2016) that reconstructs lift and drag hysteresis curves from a decomposition of the lift polars. The computational efficiency of the *LLFVW* calculations is increased through a GPU parallelization of the wake convection step via the OpenCL framework.

2.2.2 Numerical setup of *QBlade*

As it is currently not possible to include the wind tunnel walls into the *LLFVW* simulations of *QBlade*, far field simulations were conducted.

The lift and drag polar data for the rotor's *Clark-Y* airfoil is obtained through *XFOIL* (Drela and GILES, 1987) calculations ($NCrit = 9$ and forced transition at leading edge) for a range of Reynolds numbers and then extrapolated to $360°$ angles of attack using the Montgomerie method (Montgomerie, 2004).

The main simulation parameters used in the *LLFVW* simulation of this study are given in Table 2.

The azimuthal discretization of $5°$ was chosen to achieve a compromise between computational efficiency and accuracy. The wake was fully resolved for eight revolutions to obtain high quality results in rotor plane region, after which it was truncated. The blade was discretized into 21 panels in radial direction using sinusoidal spacing to obtain a higher resolution in the tip and hub regions where the largest gradients in circulation are expected. The simulation was carried out over 16 revolutions resulting in 1152 time steps and a maximum of $52,000$ wake segments. Fig. 4 shows a snapshot of the *LLFVW* simulation after four rotor revolutions.

Table 2. Main parameters of the *QBlade* simulations.

Azimuthal discretization	$5°$
Blade discretization	15 (sinusoidal spacing)
Maximum wake length	8
Simulation length	16 rev

2.3 The CFD Code *FLOWer*

2.3.1 Numerical methods of *FLOWer*

The URANS simulations are carried out using the block-structured solver *FLOWer*, which uses the finite volume method. It solves the compressible Navier-Stokes-Equations and was developed by the German Aerospace Center (*DLR*) in the course of the *MEGAFLOW* project (Kroll et al., 2000) whereas wind energy specific extensions were made at the Institute of Aerodynamics and Gas Dynamics (*IAG*) of the University of Stuttgart. For the temporal discretization, an implicit dual time stepping

Wind Energ. Sci. Discuss., https://doi.org/10.5194/wes-2017-42
Manuscript under review for journal Wind Energ. Sci.
Discussion started: 9 October 2017

eawe european academy of wind energy
Open Access WIND ENERGY SCIENCE DISCUSSIONS

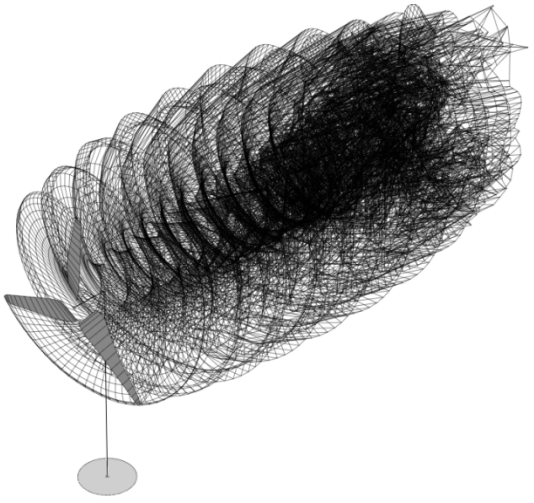

Figure 4. Snapshot of the *LLFVW* simulation after four rotor revolutions.

scheme is used (Jameson, 1991). The space is discretized with a second order central discretization scheme JST (Jameson et al., 1981). For the modelling of the turbulence, the Menter SST turbulence model is used and the simulations are performed fully turbulent. All components of the setup are meshed separately with a fully resolved boundary layer ($y^+ \approx 1$) and overlapped, using the *CHIMERA* technique (Benek et al., 1986). The process chain, as used for the present investigations, was developed at the *IAG* (Meister, 2015).

2.3.2 Numerical setup of *FLOWer*

The numerical setup consists of eleven grids (background grid (wind tunnel (WT) or far field (FF)), hub, nacelle, $3\times$connection for the blade (blade con), $3\times$blade, tower and connection for the tower (tower con)). The number of cells per grid for all cases can be found in Table 3.

Altogether, the setup in the wind tunnel has 40.1 mio cells. The case under far field condition features 38.0 mio cells.

Table 3. Cell number in mio of the individual grids for the wind tunnel and far field cases.

Wind tunnel (WT)							
Name	WT	Hub	Nacelle	Blade con	Blade	Tower con	Tower
No. of cells	11.7	2.2	1.3	0.5	7.2	0.2	1.6
Far field (FF)							
Name	FF	Hub	Nacelle	Blade con	Blade	Tower con	Tower
No. of cells	14.7	2.2	1.3	0.5	5.5	0.2	1.6

Wind Energ. Sci. Discuss., https://doi.org/10.5194/wes-2017-42
Manuscript under review for journal Wind Energ. Sci.
Discussion started: 9 October 2017

eawe european academy of wind energy
Open Access WIND ENERGY SCIENCE DISCUSSIONS

The blade is meshed automatically and is of CH-topology. The boundary layer is fully resolved with 37 grid layers, ensuring $y^+ < 1$ for the first grid layer. Around the airfoil 181 cells were used, in spanwise direction 145 cells for the wind tunnel case and 101 for the far field case. For the wind tunnel case, at around 60% of the radius and at around 90% of the radius, spanwise refinements were introduced, which ensure a proper transition for future trailing edge flap deflection. The meshes for all other components, except the far field mesh, are created manually.

The model wind turbine is placed in the settling chamber of the *GroWiKa* of the TU Berlin (Bartholomay et al., 2017), where a high blockage ratio (40%) occurs. Klein et al. (2017) already showed, that the wind tunnel walls, the tower and the nozzle behind the turbine have a significant influence on the turbine performance. Therefore, they are taken into account for the present *CFD* simulations. The $4.2 \times 4.2\mathrm{m}^2$ settling chamber begins $1.245\mathrm{m}$ upstream of the rotor plane and is $5.0\mathrm{m}$ long. As the original test section of the wind tunnel is located behind the settling chamber, in this configuration, the nozzle is located behind the "new" test section. It has a total length of $3.0\mathrm{m}$ and a tapering of 2.2. The wind tunnel walls are realized as slip walls, whereby an approximated displacement thickness, based on the turbulent flow over a flat plate, is added on the real walls. This leads to a constant reduction of the cross section over the whole settling chamber.

In order to prevent the convection of disturbances from the inflow and outflow plane of the computational domain into the measuring section, the wind tunnel was extended to a length of approximately $16.5R$, whereas the rotor plane is located after approximately $7.5R$. The cells around the turbine have an extension of $0.025 \times 0.025 \times 0.025\mathrm{m}^3$. In the direction of the inflow, the cells are stretched up to $0.4\mathrm{m}$ in x-direction, at the outflow, they measure $0.2 \times 0.025 \times 0.025\mathrm{m}^3$. The inflow boundary is realized as far field, at the outflow, a constant pressure is defined in order to maintain mass continuity.

As the wind tunnel and the nozzle could not be taken into account in *QBlade*, yet, a far field case was created, too. Thereby, the refinement for the flaps in the blade mesh was not realized. The background mesh for the far field case was created by an automated script (Kowarsch et al., 2016), which uses hanging grid nodes for the refinement. Usually, in a H-topology, the refinement is not only at the designated spot, but has to be taken along to unnecessary areas. With hanging grid nodes, refinements can be realized only where they are needed. The grid has an overall length of $20.5R$ ($8R$ upstream and $12.5R$ downstream of the rotor), a width of approximately $24.6R$ and a height of approximately $14R$. Consequently, the boundaries are, according to Sayed et al. (2015), far away enough to prevent disturbances on the solution. The boundaries, except the bottom, which is realized as slip-wall, are realized as far field boundary condition. Around the turbine, the cells have a dimension of $0.025 \times 0.025 \times 0.025\mathrm{m}^3$, at the borders $0.1 \times 0.1 \times 0.1\mathrm{m}^3$. For a one third model, a grid convergence index study according to Celik et al. (2008) was already performed (Fischer et al., 2016).

For the wind tunnel cases, the simulation was performed until convergence of the loads was achieved. This occurs when the difference between the average of torque and thrust over five revolutions and the average of the following five revolutions is $< 0.1\%$. Afterwards, the average of the last five revolutions were used for the evaluation. The temporal discretization corresponds to $1.5°$ azimuth and 100 inner iterations for the cases including wind tunnel walls and $1.5°$ azimuth with 30 inner iterations for the far field case.

Wind Energ. Sci. Discuss., https://doi.org/10.5194/wes-2017-42
Manuscript under review for journal Wind Energ. Sci.
Discussion started: 9 October 2017

eawe european academy of wind energy
Open Access WIND ENERGY SCIENCE DISCUSSIONS

2.4 Characteristics of the setups

As, according to Schepers (2012), wind turbines are exposed to yaw misalignment from 2% up to 10% of their operating time, these load cases play an important role in wind energy. Therefore, three different cases concerning the inflow direction are taken into account in the present paper. $CaseBASE$ corresponds to the turbine under uniform inflow. In $CaseYAW15$, the turbine is rotated by $-15°$ around the z-axis of the rotor plane. Usually, a turbine is rotated around the tower. However, as the model wind turbine is placed in a wind tunnel, a rotation around the tower would lead to different clearance distances of the blades to the wall for one revolution. Therefore, the turbine is rotated around the z-axis of the rotor in order to achieve a constant distance between blade tip and wind tunnel walls over a whole revolution. $CaseYAW30$ is rotated by $-30°$. The experimental results have the affix $_{Exp}$, the ones of *QBlade* $_{QBlade}$ and the *FLOWer* results are designated by $_{FLOWer}$. The far field case of *FLOWer* has the addition $_{-FF}$. Table 4 gives an overview of the different cases.

Fig. 5 shows the surfaces of $CaseBASE_{FLOWer}$ and $CaseYAW30_{FLOWer}$. There, the unusual position of the nozzle and the uncommon yaw movement become obvious.

Fig. 6 shows the position of the velocity planes, the evaluation surfaces for the *CircAve* (*LineAve* with circles) method for the AoA determination exemplary at blade 1 as well as the surfaces used for the *RAV* method of the AoA determination.

Table 4. Overview of the cases.

Wind tunnel			
Yaw	Experiment	*QBlade*	*FLOWer*
$0°$	$CaseBASE_{Exp}$	—	$CaseBASE_{FLOWer}$
$-15°$	$CaseYAW15_{Exp}$	—	$CaseYAW15_{FLOWer}$
$-30°$	$CaseYAW30_{Exp}$	—	$CaseYAW30_{FLOWer}$
Far field			
Yaw	Experiment	*QBlade*	*FLOWer*
$0°$	—	$CaseBASE_{QBlade}$	$CaseBASE_{FLOWer-FF}$
$-15°$	—	$CaseYAW15_{QBlade}$	—
$-30°$	—	$CaseYAW30_{QBlade}$	—

2.5 Data acquisition

2.5.1 Generation of the velocity planes

In the experiment, the red dots in Fig. 1 (left) at $x = -0.43d$, $x = 0.5d$ and $x = 1.05d$ indicate where hot-wire measurements are conducted. A semi-automatic traverse with four cross-wire probes with a measurement frequency of $f_s = 25\text{kHz}$ and a

Wind Energ. Sci. Discuss., https://doi.org/10.5194/wes-2017-42
Manuscript under review for journal Wind Energ. Sci.
Discussion started: 9 October 2017

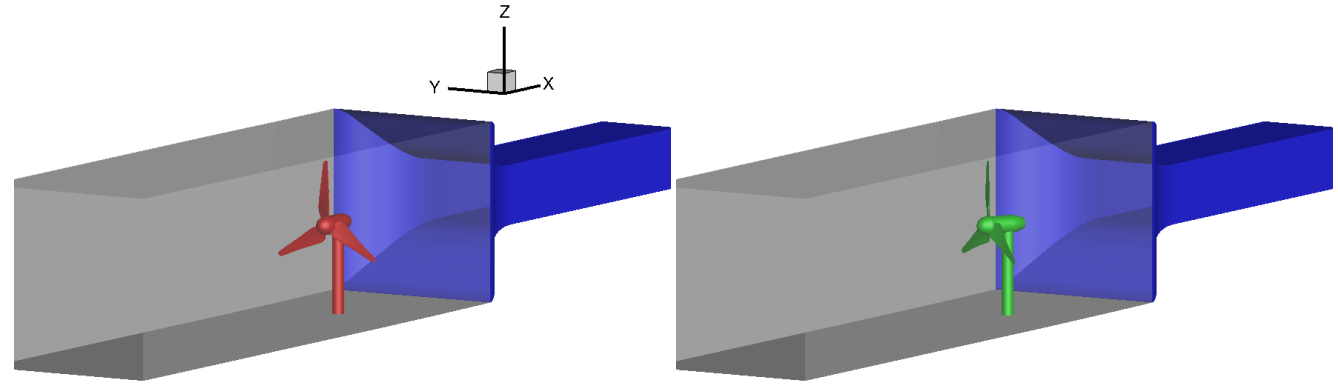

Figure 5. Surface for $CaseBASE_{FLOWer}$ (left) and $CaseYAW30_{FLOWer}$ (right).

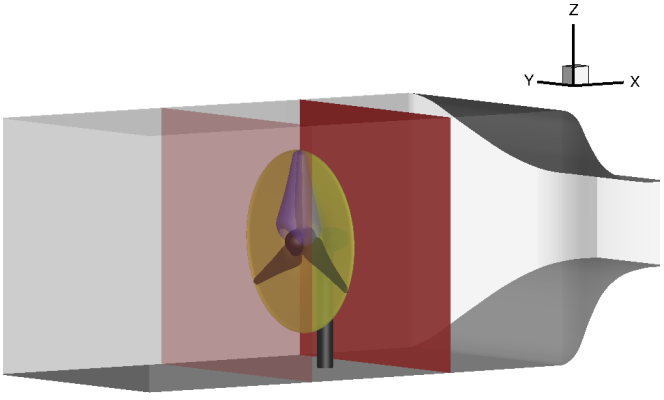

Figure 6. Position of the velocities planes for the *RAV* method (yellow), surface for the determination of the AoA with the *CircAve* method (blue) and velocity planes (red).

cut-off frequency of $f_{cut} = 10\text{kHz}$ is used. Each of the 608 measurement positions, Fig. 1 (right), in each cross-section is measured for $T_s = 16\text{s}$. Offset correction between the probes was realized by repeating multiple measurement points with all four probes.

In the *CFD* simulation, at each point of the numerical grid, data was extracted for the planes and averaged over five revolutions. In order to evaluate the differences between measurement and simulation, the results of the simulation are interpolated to a grid with the same grid points as the measurement points and the results are subtracted.

2.5.2 Extraction of the on-blade velocity and the angle of attack

The angle of attack (AoA) is the angle between the velocity, as seen by the blade (on-blade velocity) and the airfoil chord. Generally, deriving an angle of attack in rotating domain is somewhat difficult, as the AoA is a two-dimensional value. Moreover,

Wind Energ. Sci. Discuss., https://doi.org/10.5194/wes-2017-42
Manuscript under review for journal Wind Energ. Sci.
Discussion started: 9 October 2017

eawe european academy of wind energy
Open Access WIND ENERGY SCIENCE DISCUSSIONS

the blade deflects the streamtraces due to the induction of the blade and therefore changes the value of the AoA (see Fig. 7).

In the experiment the AoA and the on-blade velocity is measured by three-hole probes located at $65\%R$ and $85\%R$. The

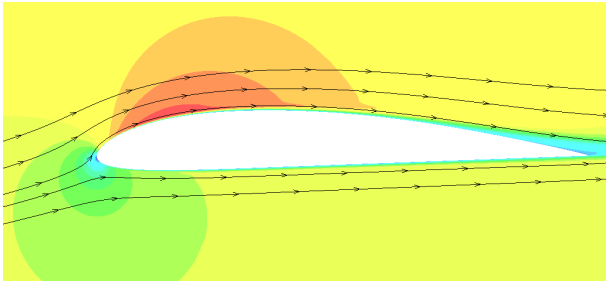

Figure 7. Deflection of the streamtraces due to the airfoil.

derivation of the section-wise values, referenced to the quarter-chord point of each section, is detailed by Bartholomay et al. (2017) and will be explained here shortly. Generally, this measurement method is advantageous, as no static tunnel reference pressure is needed and short tubing, as the pressure sensors are located in the blade, mitigates possible delay effects. The three-hole probes measure the α_{probe} and $U_{rel,probe}$ in reference to the probe position upstream of the wing. These values are derived by calibration of the pressure differences between tubes to the flow angle and velocity. However, when mounted on the wing, the results are affected by the induction of the blade and therefore need to be translated into the sectional angle of attack α and the relative velocity U_{rel}. In this project a procedure based on two dimensional flow assumption on the wing, Fig. 8, was employed.

Herein, α_{probe} is first rotated into the local coordinate system, which is based on the local chord, to derive $\alpha_{probe,section}$.

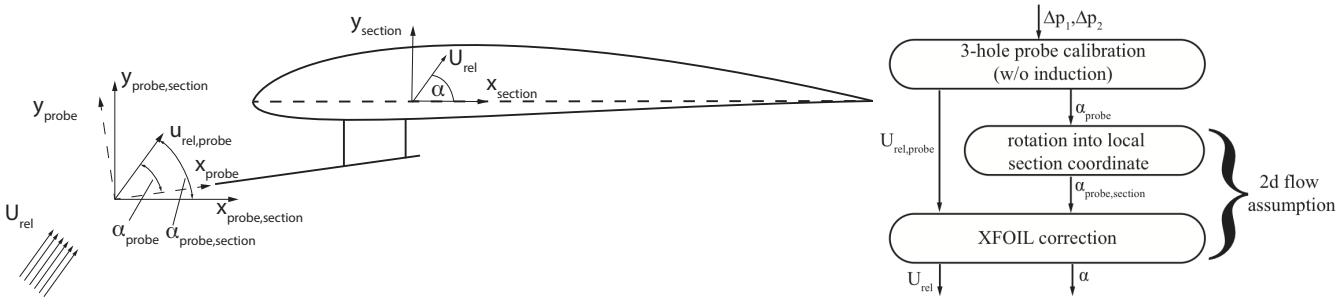

Figure 8. Schematic and flow chart of derivation of the section-wise AoA (Bartholomay et al., 2017).

Subsequently, a look-up table is used, that was derived by viscous *XFOIL* (Drela and Youngren, 2008) calculations. This table correlates the measurement at the probes head upstream of the wing to the actual local section angle of attack α. Thereby, the induction effect is accounted for and α and U_{rel} are found. However, only the circulation of the blade section, and not of the whole blade, is taken into account in this approach. The data-set was created by analyzing polars from $\alpha = -30°...30°$ in steps of $0.5°$. Steps in-between are interpolated. This procedure requires two-dimensional flow over the blade, which is

Wind Energ. Sci. Discuss., https://doi.org/10.5194/wes-2017-42
Manuscript under review for journal Wind Energ. Sci.
Discussion started: 9 October 2017

eawe european academy of wind energy
Open Access WIND ENERGY SCIENCE DISCUSSIONS

assumed to be appropriate in this case, in comparison to quantitative tuft flow analysis (Vey et al., 2015), which indicated little three-dimensional effects on the surface flow.

In *QBlade*, the angles of attack are evaluated at the quarter chord position of the airfoils at the lifting line (the bound vorticity) of the rotor blades. The angle of attack is calculated from the part of the absolute velocity vector that lies inside the respective airfoils cross sectional plane – which corresponds to the on-blade velocity. The absolute velocity vector itself is a superposition of the inflow-, relative-, wake induced- and self-induced velocity vectors.

Different methods to derive the effective sectional AoA from 3D *CFD* predicted flow fields are compared and evaluated by Jost (2017). Details of the methods will be described in a separate manuscript. The two methods, which are most suitable for the present case, are used for the AoA extraction shown in this paper. The reduced axial velocity method (herein after called *RAV*) uses two planes, one upstream and one downstream of the rotor (see Fig. 6). In these planes, the average velocities are calculated and afterwards the velocity components are used to determine the velocity in the rotor plane without the induction of the blade. The method was developed by Klein (2017) based on the method of Johansen and Sørensen (2004), who determined airfoil characteristics from 3d *CFD* rotor computations. It was successfully applied by Jost et al. (2016) to investigate unsteady 3d effects on trailing edge flaps, and by Klein et al. (2014) for *CFD* analysis of a 2-bladed multi-megawatt turbine. In the line averaging method (*LineAve* or *CircAve*), which was developed by Jost (2017), the AoA is determined by averaging the velocity over a closed line around each blade cut (see Fig. 6). For both approaches, the results are averaged over five revolutions.

2.5.3 Determination of the bending moments

In the present paper, the flapwise (out-of plane) moment (M_y) and the edgewise (in plane) moment (M_x) are investigated. Experimentally, a full-bridge strain-gauge setup is employed for each bending moment. The strain-gauges are glued on the bolt, Fig. 3, that connects the blades to the hub. The full-bridge aims to mitigate cross-talk effects that influence the measurement results. Nonetheless, as positioning of the strain gauges on the circular bolt is challenging, cross-talk effects are present on the results of the sensors. The main sources of cross-talk are bending moments of edgewise on the flapwise sensor and vice versa, axial forces due to weight and centrifugal acceleration, but they can also be caused by the blade twist. The first two effects are quantified by calibration and compensated for in the measurements. The herein presented results are low-pass filtered at $f_{cut} = 15\text{Hz}$ and notch-filtered at $4p$.

In the *LLFVW* method of *QBlade* the blade bending moments are evaluated by summing up the elemental blade forces, obtained from an integration of the normal and tangential forces along the blade span that are obtained via the stored airfoil coefficients.

In the *CFD* simulation, the bending moments in the blade root result from the pressure and friction on the blade surface. For each surface cell the forces are computed and multiplied with the corresponding radius. Then, they are averaged over five revolutions.

Wind Energ. Sci. Discuss., https://doi.org/10.5194/wes-2017-42
Manuscript under review for journal Wind Energ. Sci.
Discussion started: 9 October 2017

eawe european academy of wind energy
Open Access WIND ENERGY SCIENCE DISCUSSIONS

3 Results and discussion

3.1 Comparison of the velocity planes

The velocity planes, which are taken into account in the present study, are placed $0.43D$ upstream and $0.5D$ downstream of the rotor plane (see Fig. 6).

Fig. 9 (left) shows the velocity in x-direction for the measurement and at the right picture for the *FLOWer* wind tunnel simulation $0.43D$ upstream of the rotor plane. The measuring points are shown as black dots. The dimensions of the wind tunnel, as well as the model wind turbine, are illustrated by dashed lines. Moreover, an isoline with the undisturbed inflow velocity of $6.5\mathrm{m/s}$ is shown.

The turbine blockage effect can be observed in both figures. However, the velocity distribution in the simulation is smoother

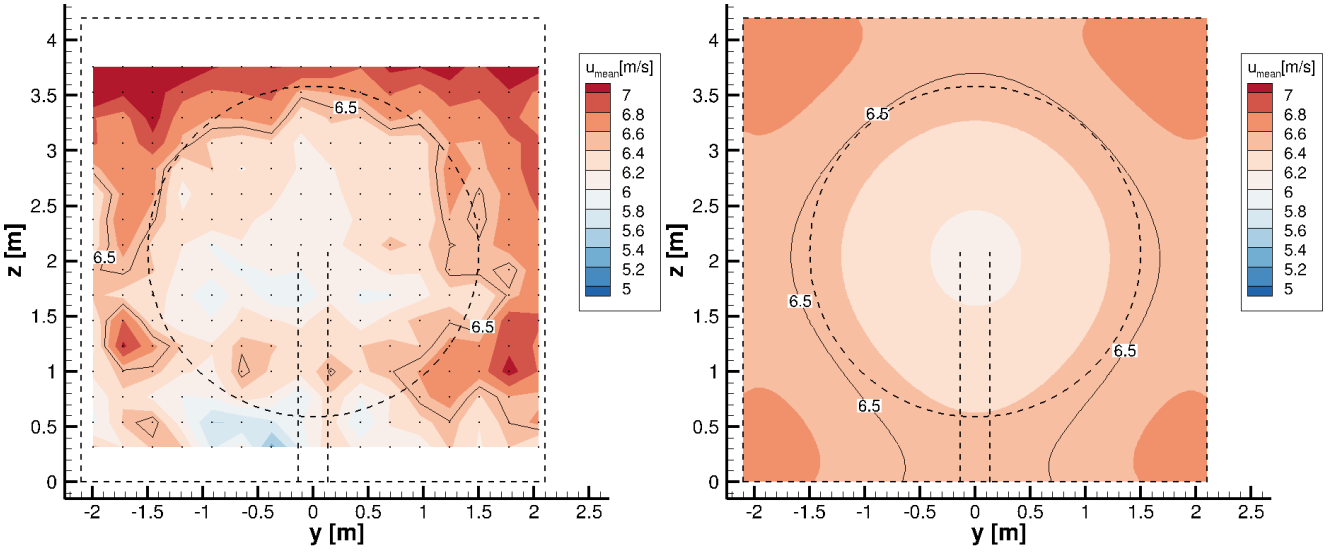

Figure 9. : Hot-wire measurements (left) and simulated velocity plane (right) of the x-velocity $0.43D$ upstream of the rotor plane. The dashed lines illustrate the wind tunnel and the turbine. Isolines show the undisturbed inflow velocity of $6.5\mathrm{m/s}$. The dots in the left figure show the discrete measuring points.

and axisymmetric, leading to a clearly defined blockage, whereas it is more frayed in the experiment. In the measurement an increase of the velocity can be seen over the whole ceiling of the test section and a decrease at the bottom whereas in the simulation, a slightly higher velocity can be seen in the corners of the wind tunnel.

In the experiment, multiple causes of possible measurement errors, such as temperature compensation or induction of the traversing system are analyzed and ruled out. Therefore, the horizontal inequalities seem to result from the design of the wind tunnel. More information about this topic can be found in (Bartholomay et al., 2017).

In Fig. 10, the relative difference between simulation and measurement with regard to the mean inflow velocity of 6.5m/s is shown.

Wind Energ. Sci. Discuss., https://doi.org/10.5194/wes-2017-42
Manuscript under review for journal Wind Energ. Sci.
Discussion started: 9 October 2017

The differences between both velocity planes are small and except for a small area at the bottom of the wind tunnel, lower

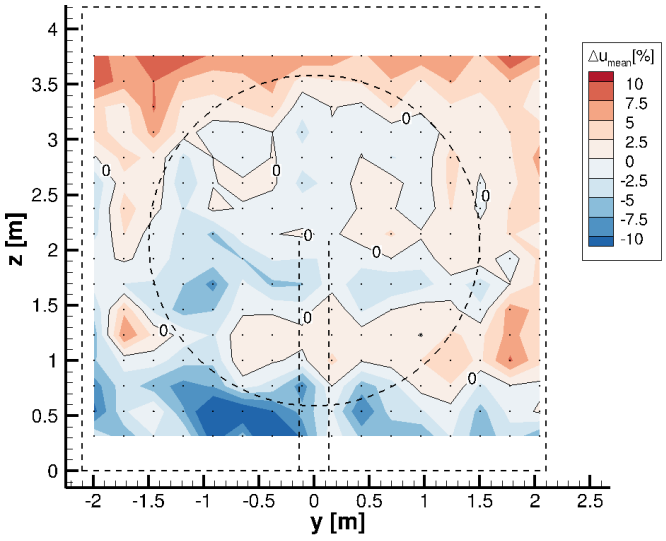

Figure 10. Relative velocity difference between measurement and simulation with regard to the undisturbed inflow velocity of $6.5\mathrm{m/s}$, $0.43D$ upstream of the rotor plane. The dashed lines illustrate the wind tunnel and the turbine. Isolines show 0% deviation. The dots show the discrete evaluation points.

than $\pm 10\%$ of the inflow velocity, which corresponds to $\pm 0.65\mathrm{m/s}$.

Fig. 11 (left) shows the velocity in x-direction for the measurement and at the right picture for the simulation $0.5D$ downstream of the rotor plane. Again, the measuring points are indicated by black dots, the dimensions of the wind tunnel and the model wind turbine by dashed lines. An isoline with the mean velocity of $6.5\mathrm{m/s}$ is shown, too.

Some aspects, as already seen upstream of the rotor (Fig. 9), are also apparent downstream of the rotor. In both figures (left and right), the wake of the rotor, indicated by lower velocity, can be seen clearly. Around the rotor, as a result of limited space due to the wind tunnel walls, higher velocities are achieved. Again, in the experiment, the velocity at the upper part of the wind tunnel is slightly higher then at the bottom. As the *GroWiKa* is a closed loop wind tunnel, the turbulence intensity in the wind tunnel is higher than in the simulation. This missing turbulence in the simulation might be the reason why the border of the rotor wake is almost a perfect circle in the right picture, whereas it is more smeared in the measurement. Moreover, the decay of the tip vortices has not yet started so shortly behind the rotor plane. As the simulation has a finer resolution, the velocity distribution is smoother there. In the simulation, there is a stronger velocity deficit in the wake of the nacelle. This can have several reasons. In the simulation, the missing inflow turbulence might have an effect on the stability of the wake, but is certainly not the main reason for the deviation. In the experiment, the boundary layer of the nacelle is not tripped, whereas a fully turbulent approach is used in the simulation. These differences concerning the boundary layer of the nacelle might lead to a different recovery of the wake of the nacelle. Due to the flow separation on the nacelle, the flow in the wake of the nacelle is highly unsteady and the main flow direction is not clearly defined (angles larger than $\pm 60°$ occur in the simulation), whereby

Wind Energ. Sci. Discuss., https://doi.org/10.5194/wes-2017-42
Manuscript under review for journal Wind Energ. Sci.
Discussion started: 9 October 2017

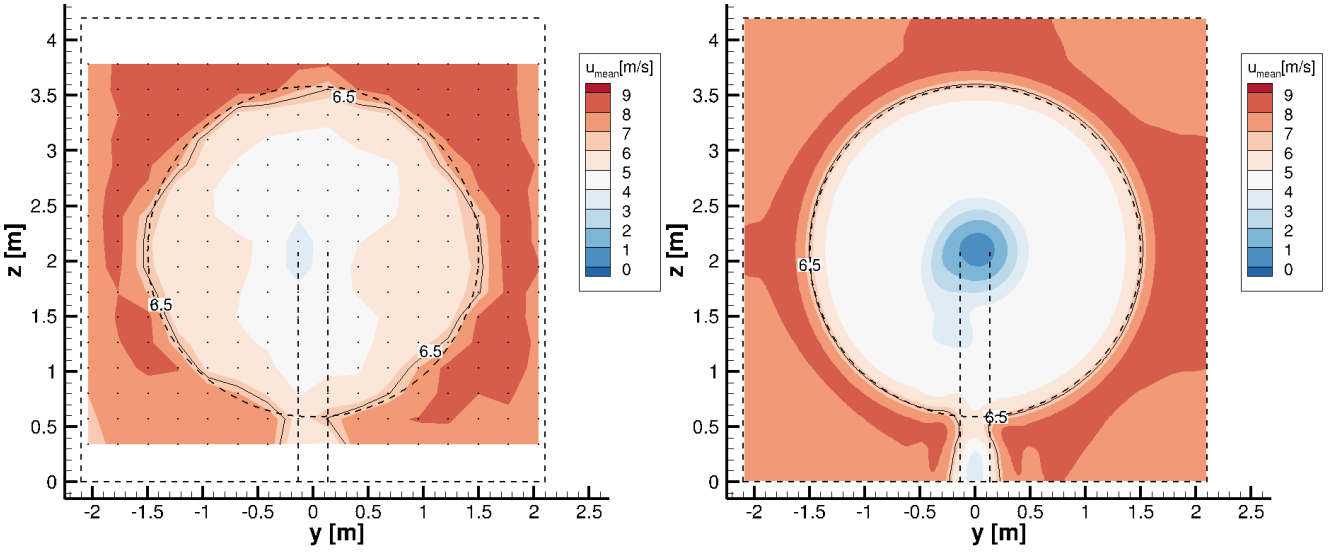

Figure 11. Hot-wire measurements (left) and simulated velocity plane (right) of the x-velocity $0.5D$ downstream of the rotor plane. The dashed lines illustrate the wind tunnel and the turbine. Isolines show the mean inflow velocity of $6.5\mathrm{m/s}$. The dots in the left figure show the discrete measuring points.

proper working conditions of the x-wire probe are no longer guaranteed. Therefore, the measured x-component of the velocity is influenced by the y- and z-component, which could also lead to deviations between measurement and simulation.

Fig. 12 shows the relative difference between simulation and measurement with regard to the mean inflow velocity of 6.5m/s. It can be seen, that except for the wake of the nacelle and some tip vortices, the differences between simulation and measurement are again below 10%.

All things considered, the accordance between experiment and simulation is quite good as they are, except for some parts in the outer region of the rotor and in the wake of the nacelle, smaller than $\pm 0.65\mathrm{m/s}$.

3.2 Analysis of the on-blade velocity

Hereinafter, the on-blade velocity, meaning the velocity seen by the blade section at a distinct radial position, for $CaseBASE$ for experiment, *QBlade* and *FLOWer* (both methods *RAV* and *CircAve*) are displayed at two different rotor locations (65% and 85%) over the azimuth (Fig. 13), whereas an azimuth of $0°$ corresponds to the top position of the first blade.

At 65%R, the simulations overestimate the velocity slightly, but at 85%R there is a good accordance between the simulation results and the experiment. The higher fluctuations in the experiment at the outer radial position might be a result of a vibration of the mounting of the probe. For both radial positions, all simulations match well. For the *FLOWer* simulations, both methods (*RAV* and *CircAve*) have the same results. In the outer part of the blade, the on-blade velocity is dominated by the tangential velocity. Consequently, both *FLOWer* setups (wind tunnel and far field), show almost the same results, too.

Wind Energ. Sci. Discuss., https://doi.org/10.5194/wes-2017-42
Manuscript under review for journal Wind Energ. Sci.
Discussion started: 9 October 2017

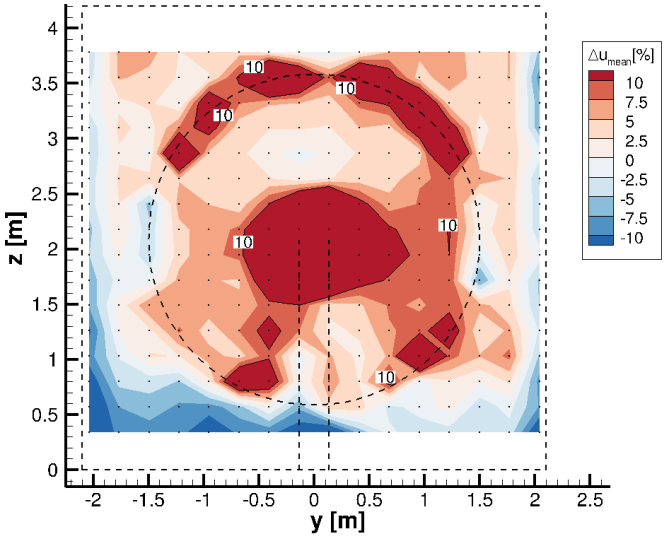

Figure 12. Relative velocity difference between measurement and simulation with regard to the undisturbed inflow velocity of $6.5\mathrm{m/s}$, $0.5D$ downstream of the rotor plane. The dashed lines illustrate the wind tunnel and the turbine. Isolines show 10% deviation. The dots show the discrete evaluation points.

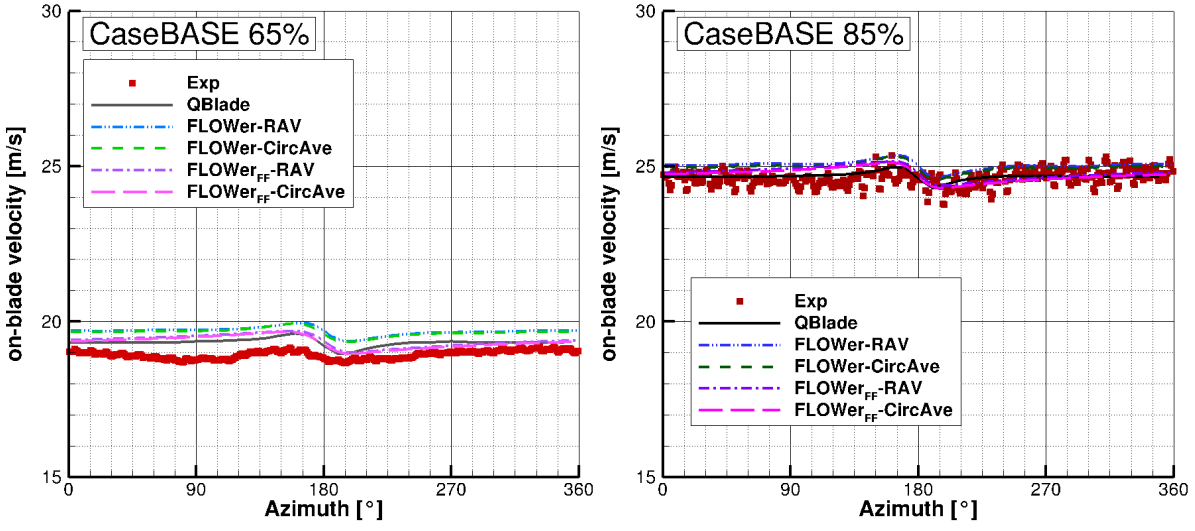

Figure 13. On-blade velocity distribution over azimuth for $CaseBASE$ for the experiment, *QBlade* and *FLOWer* (*RAV* and *CircAve* for wind tunnel and FF each) at $65\%R$ (left) and $85\%R$ (right).

The influence of the tower blockage around an azimuth of $180°$ can be seen at both radial positions as a small increase before the tower passage and a small drop afterwards. The increase of the inflow velocity is due to the displacement effect of the tower. Directly upstream of the tower, the velocity is reduced until it has recovered shortly afterwards. Except for this drop, the

Wind Energ. Sci. Discuss., https://doi.org/10.5194/wes-2017-42
Manuscript under review for journal Wind Energ. Sci.
Discussion started: 9 October 2017

velocity is almost constant over the whole revolution.

Fig. 14 shows the velocity over azimuth under yaw=$-15°$.

As the wind tunnel walls should not be neglected in the present setup, a far field case under yawed condition for *FLOWer* was

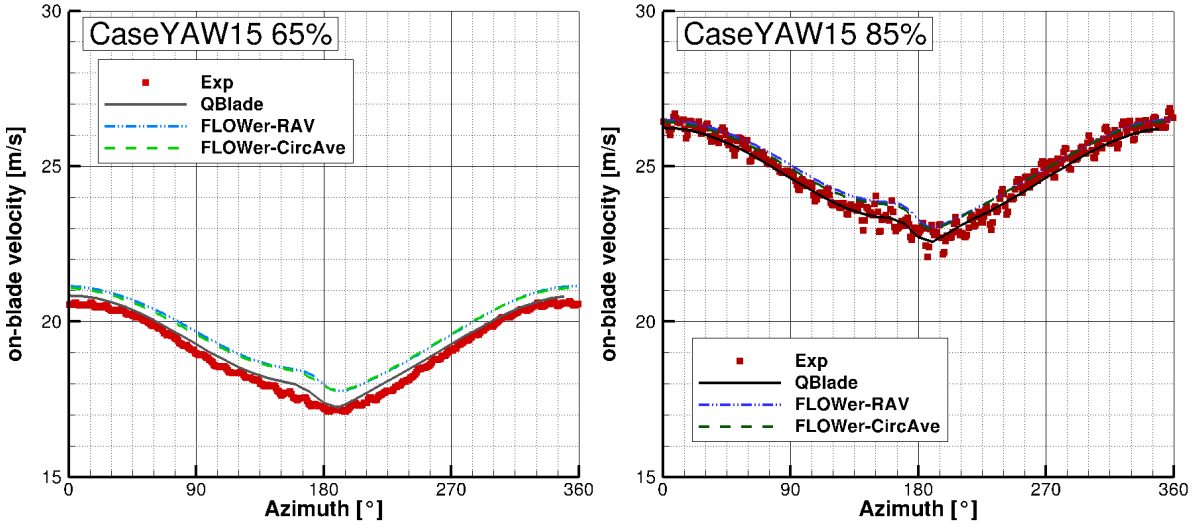

Figure 14. On-blade velocity distribution over azimuth for $CaseYAW15$ for the experiment, *QBlade* and *FLOWer* (*RAV* and *CircAve*) at $65\%R$ (left) and $85\%R$ (right).

not simulated. At 65%R, the experimental and *QBlade* results are almost identical, whereas *FLOWer* predicts a slightly higher velocity ($\approx 0.5\mathrm{m/s}$). At 85%R, there is still a small offset between *QBlade* and *FLOWer*, but the measurement lies between the two curves. The influence of the tower is covered by the influence of the yaw misalignment, which leads to stronger variations over one revolution. In the upper part of the rotor (azimuth=270°-90°), the blade is advancing, while it is retreating in the lower part (azimuth=90°-270°). This leads to a $1p$ variation of inflow velocity as seen by the blade. More information about yaw misalignment and its effects can be found in Schulz et al. (2017), where the impact of yawed inflow on loads, power and near wake of a generic wind turbine was analyzed.

In Fig. 15, where the velocity over azimuth under yaw=$-30°$ is plotted, the influence of the yaw misalignment is even more pronounced.

Almost the same characteristics as already mentioned with regard to Fig. 14 can be found for $-30°$ yaw misalignment. However, at 65%R, the *FLOWer* results have a better agreement with the experiment in the upper part of the rotor whereas the *QBlade* solution has a better agreement in the lower part. At 85%R all curves correspond well.

Wind Energ. Sci. Discuss., https://doi.org/10.5194/wes-2017-42
Manuscript under review for journal Wind Energ. Sci.
Discussion started: 9 October 2017

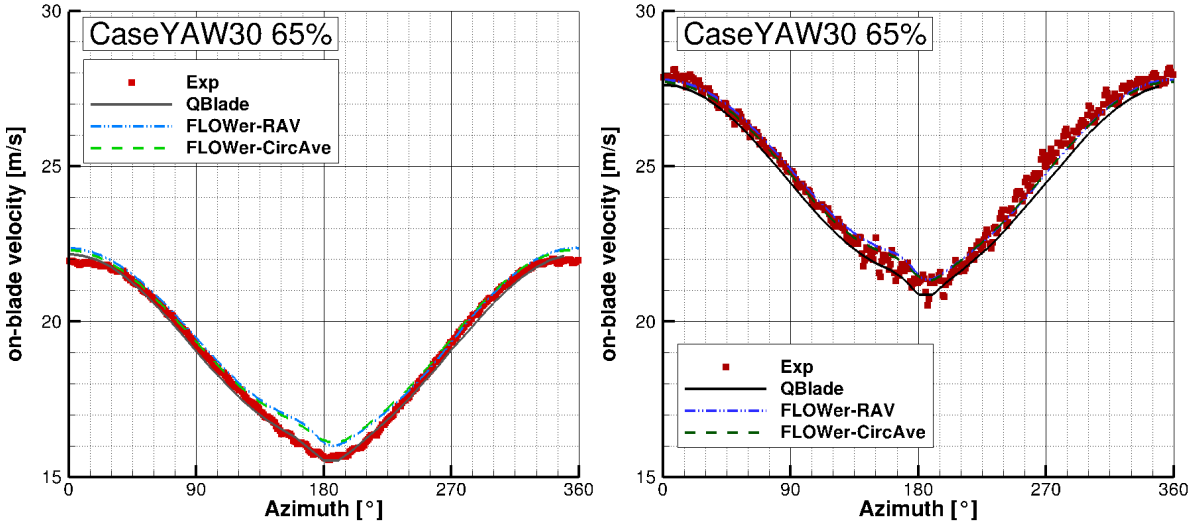

Figure 15. On-blade velocity distribution over azimuth for $CaseYAW30$ for the experiment, *QBlade* and *FLOWer* (*RAV* and *CircAve*) at $65\%R$ (left) and $85\%R$ (right).

3.3 Evaluation of the angle of attack

As for the on-blade velocity, in the following, the AoA for $CaseBASE$ for experiment, *QBlade* and *FLOWer* (both methods *RAV* and *CircAve*) are displayed at two different rotor locations (65% and 85%) over the azimuth (Fig. 16).

The tower blockage effect can be clearly seen at azimuth=$180°$, where the AoA has a drop of approximately $1°$. The influence of the tower is very distinct, due to its relative large diameter, compared to the other components of the turbine. For both, *QBlade* and *FLOWer*, the curve is almost constant before and after this drop. The dip in the experiment at approximately $90°$ azimuth is a result from the traverse, which was located in the test section upstream of the rotor. There is a good accordance between the experiment and the *FLOWer* results. Both AoA evaluation methods for the *FLOWer* solution show almost the same distribution, especially at 85%. Reasons for the differences can be attributed to the different approach of the methods (*RAV* is averaging over time and *CircAve* has a local approach). More information and reasons for the deviations can be found in (Jost, 2017). At 65%, the level of the AoA is approximately $0.5°$ lower than further outboard for experiment, *QBlade* and *FLOWer*. A constant offset of approximately $2°$ between the simulation results of *QBlade* and *FLOWer* is present for both radial positions. This is a result of the neglection of the wind tunnel walls in the *QBlade* simulation. Schümann et al. (2013) showed, that for a blockage ratio, which is defined as the rotor swept area divided by the wind tunnel cross section area, smaller than 10%, no blockage effect should be experienced and the wind tunnel walls can be neglected. However, in the present case, the blockage ratio amounts 40% and the minimal distance between blade tip and wall $0.6\mathrm{m}$. Fischer et al. (2016) showed for a one third model of the turbine a high influence of the wind tunnel walls for a wind tunnel with the same minimal distance between blade tip and wall as in reality and Klein et al. (2017) showed for the full model of *BeRT* in the *GroWiKa* an increase of 25%

Wind Energ. Sci. Discuss., https://doi.org/10.5194/wes-2017-42
Manuscript under review for journal Wind Energ. Sci.
Discussion started: 9 October 2017

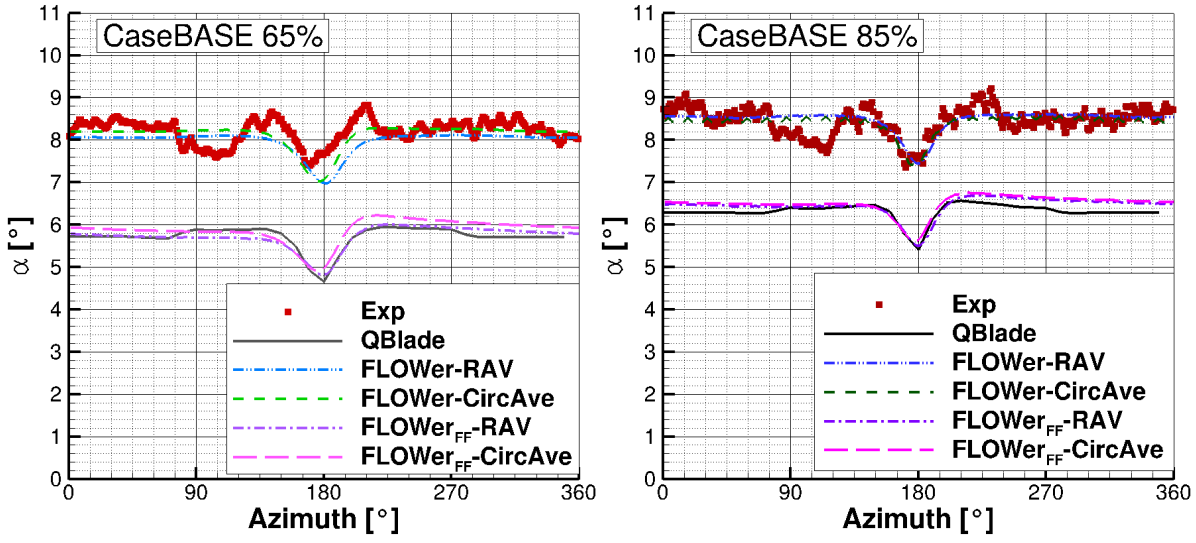

Figure 16. AoA distribution over azimuth for $CaseBASE$ for the experiment, *QBlade* and *FLOWer* (*RAV* and *CircAve* for wind tunnel and FF each) at $65\%R$ (left) and $85\%R$ (right).

in thrust and even 50% in power due the wind tunnel walls. A comparison between the *QBlade* results and the *FLOWer* results under far field condition verifies this assumption, as the distributions are almost identical.

A comparison of the AoA distribution calculated by *QBlade* and *FLOWer* over the normalized radius at azimuth=$0°$ for the wind tunnel and far field case is shown in Fig. 17.

Again, the influence of the wind tunnel can be seen in the constant offset between the two *FLOWer* cases. As already seen in Fig. 16, the offset between the *RAV* and the *CircAve* results amounts $\approx 0.15°$ for the far field case. For the wind tunnel case, the offset decreases with increasing radius. Reasons for these differences can be found in (Jost, 2017). Between approximately 40% and 90% of the radius, there is a good accordance between the *QBlade* and the *RAV* solution of the *FLOWer* far field case. Fig. 18 shows the AoA over azimuth under yaw=$-15°$.

The same characteristics as under yaw=$0°$ can also be seen in Fig. 18 under yaw=$-15°$. Again, the influence of the tower blockage is clearly visible. Unlike in $CaseBASE$, the AoA is not constant before and after the drop caused by the tower, due to the yaw misalignment.

As in $CaseBASE$, the *FLOWer* results show a good agreement to the measurements at both radial positions. The two different evaluation methods for *FLOWer* show almost the same results, too. The difference between the two radial positions amounts approximately $1°$ for all setups. The offset between *QBlade* and *FLOWer* amounts between $1.5°$ and $2°$ and is therefore again attributed to the influence of the wind tunnel walls. As already mentioned, a far field case under yaw misalignment for *FLOWer* was not simulated.

In Fig. 19 the AoA distribution over azimuth for a yaw misalignment of $-30°$ can be seen.

The effect of the tower blockage is still visible. The effects caused by the yaw misalignment are more pronounced here.

Wind Energ. Sci. Discuss., https://doi.org/10.5194/wes-2017-42
Manuscript under review for journal Wind Energ. Sci.
Discussion started: 9 October 2017

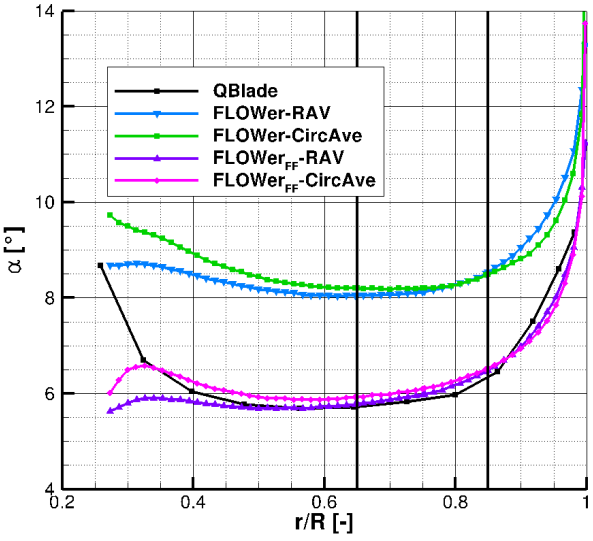

Figure 17. AoA distribution over the normalized blade radius at azimuth=0° for *QBlade* and *FLOWer* (*RAV* and *CircAve* for wind tunnel and FF each). Black lines indicate the evaluation positions of Fig 16, Fig 18 and Fig 19.

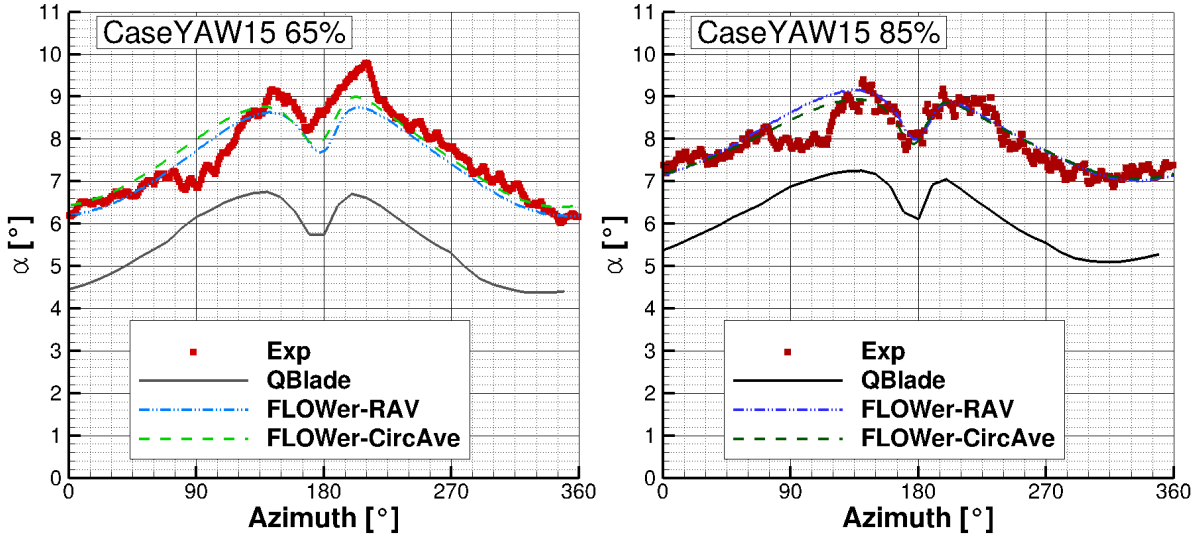

Figure 18. AoA distribution over azimuth for $CaseYAW15$ for the experiment, *QBlade* and *FLOWer* (*RAV* and *CircAve*) at $65\%R$ (left) and $85\%R$ (right).

At 65%, there is a difference between the measurement and *FLOWer* results at the downward moving blade (azimuth=0°-180°), probably due to the traverse placed in the wind tunnel, whereas there is a good agreement at the upward moving blade (azimuth=180°-360°). Further outboard, the curves correspond very well over the whole revolution, except for the dip at 90°

Wind Energ. Sci. Discuss., https://doi.org/10.5194/wes-2017-42
Manuscript under review for journal Wind Energ. Sci.
Discussion started: 9 October 2017

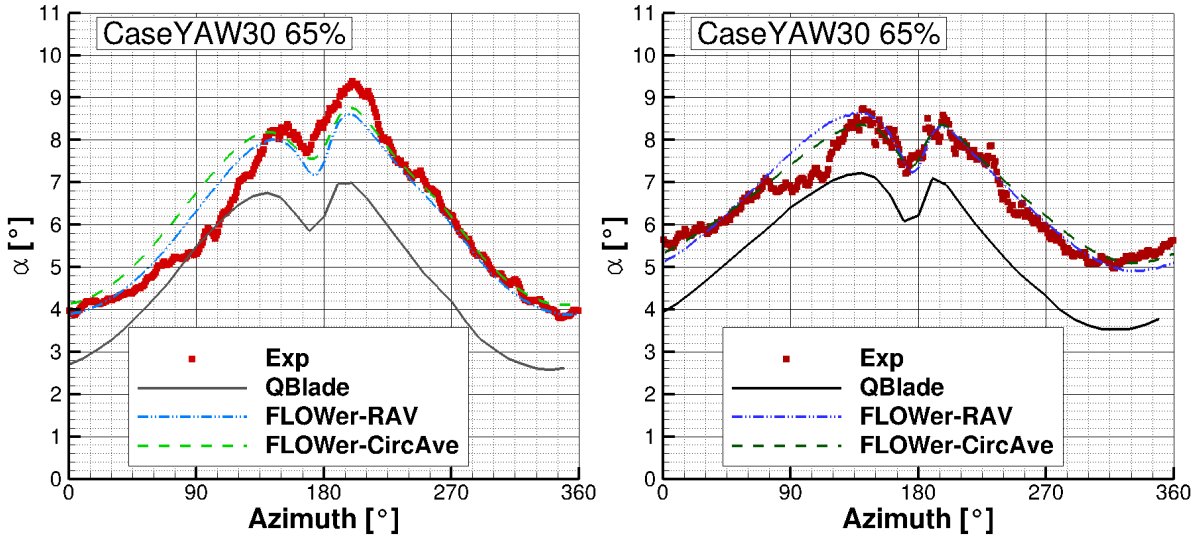

Figure 19. AoA distribution over azimuth for $CaseYAW30$ for the experiment, *QBlade* and *FLOWer* (*RAV* and *CircAve*) at $65\%R$ (left) and $85\%R$ (right).

azimuth. The offset between *QBlade* and *FLOWer*, due to the missing wind tunnel walls in *QBlade*, has decreased and amounts now approximately $1.5°$.

For all three cases ($CaseBASE$, $CaseYAW15$ and $CaseYAW30$) at both radial positions, despite the constant offset to the *QBlade* results, the amplitude and phase of the AoA of experiment, *QBlade* and *FLOWer* have a good agreement.

3.4 Investigation of the bending moments

In the *QBlade* and *FLOWer* simulations, all blades are identical, whereas in the experiment, the turbine is equipped with two baseline blades and one smart blade. However, for the current study, the flaps are fixed in their neutral position (see Sect. 2.1.3) and consequently, all three blade should have the same shape.

In the following, the measured flapwise bending moments (out-of plane, M_y) of one baseline blade and the smart blade are compared to the *QBlade* and *FLOWer* results of one arbitrary blade for all three cases. Fig. 20 shows the comparison for $CaseBASE$ (upper left), $CaseYAW15$ (upper right) and $CaseYAW30$ (lower middle). As the forces and moments mainly depend on the AoA, the same characteristics (tower shadow, influence of yaw misalignment,...) like in Fig. 16, Fig. 18 and Fig. 19, respectively, can be seen in Fig. 20, as they cascade down from the AoA to the loads.

The offset between the two *FLOWer* results for the baseline case (upper left figure) represents the influence of the wind tunnel walls. This time, the accordance between the *QBlade* results and the *FLOWer* wind tunnel case is better than between the *QBlade* case and the *FLOWer* far field case. This unexpected result might be a result of the choice of the *XFOIL* polars used for the present *QBlade* simulations, because although the AoA are similar between *QBlade* and $CaseBASE_{FLOWer-FF}$ (see

Wind Energ. Sci. Discuss., https://doi.org/10.5194/wes-2017-42
Manuscript under review for journal Wind Energ. Sci.
Discussion started: 9 October 2017

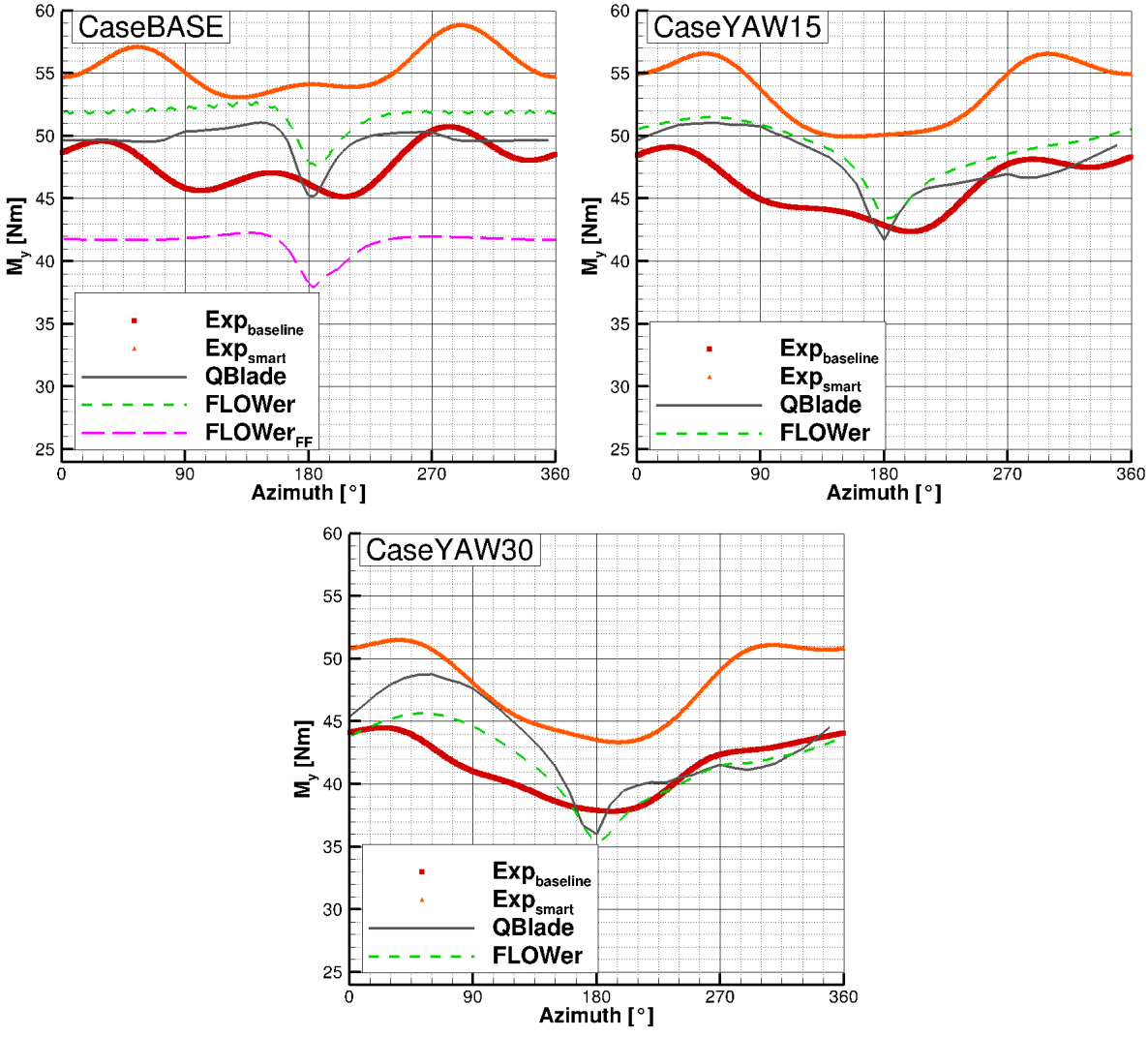

Figure 20. Flapwise bending moment (M_y) over azimuth for $CaseBASE$ (upper left), $CaseYAW15$ (upper right) and $CaseYAW30$ (lower middle) for experiment, *QBlade* and *FLOWer*.

Fig. 16), the bending moments differ.

As the experimental results are filtered (see Sect. 2.5.3), the tower shadow is less pronounced than in the simulation results. The amplitude and phase of the $1p$ frequency, caused by the yaw misalignment, show a good accordance between all curves.

The offset between the measurement results for the two blades can have several reasons. The different measurement equipment installed on the blades (see Sect. 2.1.3) might have a small influence the flow around the blade, which would have a direct effect on the loads. The surface roughness varies between the blades, which might influence the boundary layer of the blade. Although the flaps are installed in a neutral position, it can not be ruled out that a small deflection angle is present, changing

Wind Energ. Sci. Discuss., https://doi.org/10.5194/wes-2017-42
Manuscript under review for journal Wind Energ. Sci.
Discussion started: 9 October 2017

eawe european academy of wind energy
Open Access WIND ENERGY SCIENCE DISCUSSIONS

the camber and therefore the aerodynamic properties of the smart blade. A possible evidence for this assumption is the fact, that the simulated curves lie closer to the measured curves of the baseline blade than to the ones of the smart blade. In the simulation, the blades are rigid, whereas they have a certain deformation in reality. However, as the blades are short and stiff, this effect is assumed to be very small.

The comparison of the edgewise bending moments (in plane, M_x) can be found in Fig. 21. The curve for the baseline blade is missing in the current plot as the sensors had a malfunction during the measurement.

The same characteristics of the curves as for the flapwise bending moments (see Fig. 20) can also be found in the edgewise

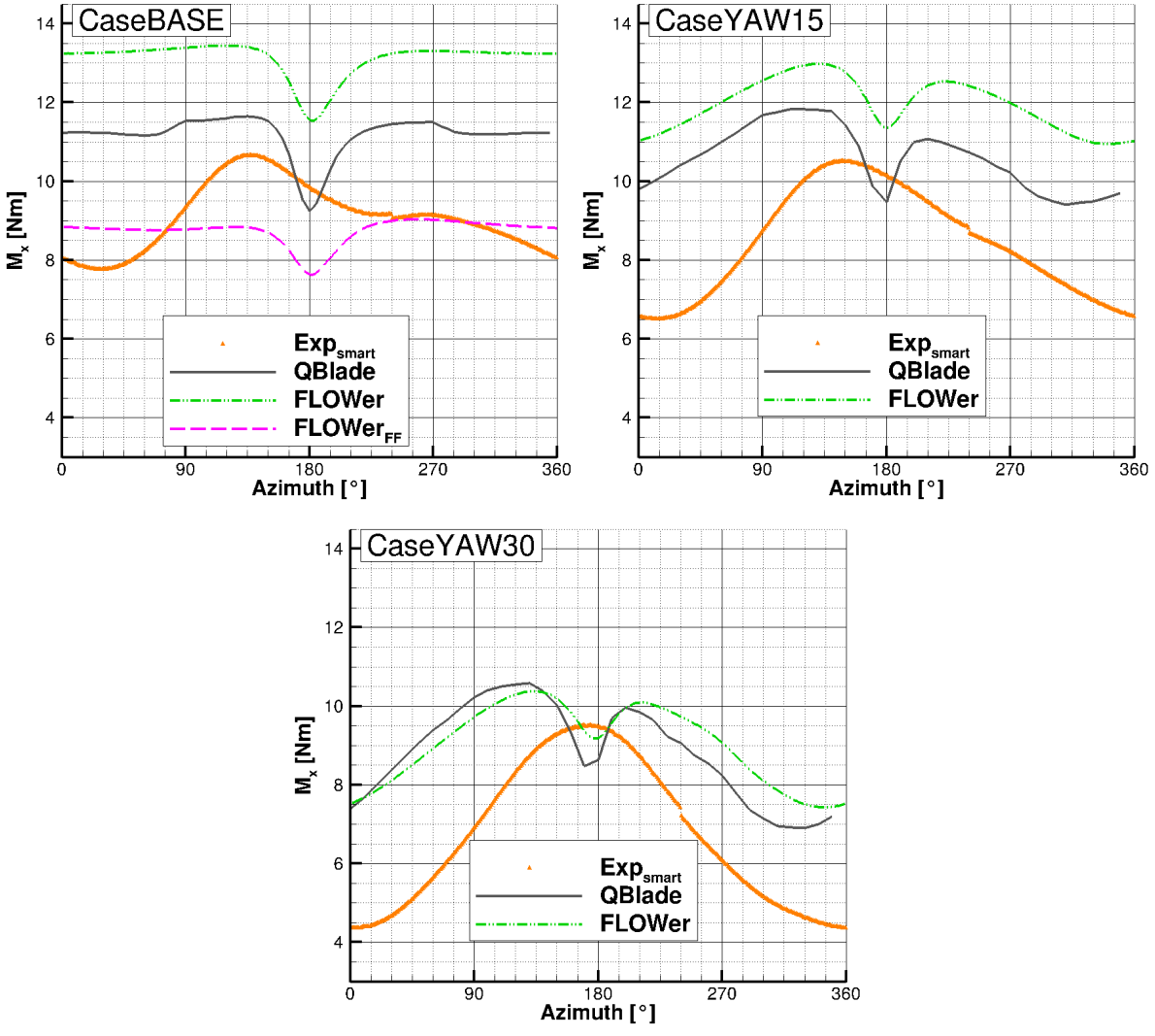

Figure 21. Edgewise bending moment (M_x) over azimuth for $CaseBASE$ (upper left), $CaseYAW15$ (upper right) and $CaseYAW30$ (lower middle) for experiment, *QBlade* and *FLOWer*.

Wind Energ. Sci. Discuss., https://doi.org/10.5194/wes-2017-42
Manuscript under review for journal Wind Energ. Sci.
Discussion started: 9 October 2017

bending moments. However, for M_x, there are bigger relative differences between all curves. For $CaseBASE$, the *QBlade* results lie in between the two *FLOWer* cases. The deviations between *QBlade* and *FLOWer* decrease with increasing yaw misalignment. All simulation curves (except the *FLOWer* far field case), overestimate the edgewise bending moments.

4 Summary

In the present paper, results from experiments of a model wind turbine placed in a wind tunnel with high blockage ratio are used for the validation of the setups of two different numerical codes, the Lifting Line Free Vortex Wake (*LLFVW*) code *QBlade* and the *CFD* code *FLOWer*. In *QBlade*, the wind tunnel walls are neglected whereby in *FLOWer*, a far field case, as well as simulations including the wind tunnel environment, are investigated. Besides code validation, the results are used to study the impact of the wind tunnel blockage effect on the blade aerodynamics. Different yaw angles are considered and examined.

A comparison of flow fields upstream and downstream of the turbine from experiment and the *CFD* code *FLOWer* show good agreement (relative difference most time under 10% inflow velocity). This is a good prerequisite for the validation of the on-blade velocity and the angle of attack, which are a result of the flow around the turbine.

For the investigation of these parameters, three different yaw cases (yaw=$0°$; $-15°$ and $-30°$) were compared between experiment, *QBlade* and *FLOWer*. Concerning the on-blade velocity, all curves are almost identical at 85% of the radius whereas there are small differences between the *FLOWer* simulations and experiment at 65%R. For the AoA, the *FLOWer* results show a very good agreement with the experimental results. The constant offset of $1°$-$2°$ between the results of the *LLFVW* code and the *CFD* code are a results of the neglection of the wind tunnel walls in the *QBlade* setup.

Finally, the blade root bending moments are compared between experiment, *QBlade* and *FLOWer*. The effect of the tower is, due to the filters, not present in the experimental results. For the out-of plane bending moment, the offset between the two *FLOWer* cases (far field and wind tunnel) is clearly visible. The accordance between the amplitude and phase of the measured curves and the simulated curves of *QBlade* and *FLOWer* is good. The offset of the predicted moment to the measured curve of the smart blade might be a result of the measuring equipment, installed on the blade, the different surface roughness and a possible deviation of the position of the flaps from neutral position. The edgewise bending moment shows bigger relative deviations and the simulations overestimate the loads.

To sum up, a good accordance was achieved between experiment and *FLOWer* and consequently the numerical setup of *FLOWer* can be seen as validated in terms of flow fields, on-blade velocity, AoA and bending moments. Therefore, it can be used for further investigations. Concerning the *QBlade* results, the on-blade velocity, as well as the amplitude and phase of the AoA and the bending moments can be seen as validated by the experiment. As the AoA distribution of *QBlade* lies on the far field solutions of *FLOWer*, the differences in the mean values of the AoA can be attributed to the absence of wind tunnel walls in the *QBlade* predictions.

In a next step, experiments with passive and active load control will be performed and compared to simulations of both, *QBlade* and *FLOWer*. Thereby, *QBlade* will be used for dimensioning purposes of the flaps prior to the experiments. Afterwards, the

most promising configurations will be investigated numerically on a full size turbine by *QBlade* and *FLOWer*, where the *LLFVW* code can be used for the preliminary design, and the *CFD* code for the closer look into the aerodynamic details.

Data availability. Measurement data and simulation results can be provided by contacting the corresponding author or Thorsten Lutz (lutz@iag.uni-stuttgart.de).

Competing interests. The authors declare that they have no conflict of interest.

Acknowledgements. All computational resources used for the *FLOWer* simulations were provided by the High Performance Computing Center Stuttgart (*HLRS*). The studies presented in this article have been funded by the *German Research Foundation* (*DFG*) and were performed in the course of the *DFG* PAK 780 project.

Wind Energ. Sci. Discuss., https://doi.org/10.5194/wes-2017-42
Manuscript under review for journal Wind Energ. Sci.
Discussion started: 9 October 2017

eawe european academy of wind energy
Open Access WIND ENERGY SCIENCE DISCUSSIONS

References

Bak, C., Madsen, H. A., and Johansen, J.: Influence from blade-tower interaction on fatigue loads and dynamics (poster), in: 2001 European Wind Energy Conference and Exhibition (EWEC'01), pp. 394–397, WIP Renewable Energies, 2001.

Bartholomay, S., Fruck, W.-L., Pechlivanoglou, G., Nayeri, C. N., and Paschereit, C. O.: Reproducible Inflow Modifications for a Wind Tunnel Mounted Research HAWT, in: ASME TURBO EXPO, Charlotte, NC, USA., 2017.

Benek, J. A., Steger, J. L., Dougherty, F. C., and Buning, P. G.: in: Chimera. A Grid-Embedding Technique., 1986.

Celik, I. B., Ghia, U., Roache, P. J., et al.: Procedure for estimation and reporting of uncertainty due to discretization in {CFD} applications, Journal of fluids {Engineering-Transactions} of the {ASME}, 130, https://doi.org/10.1115/1.2960953, 2008.

Drela, M. and GILES, M.: Viscous-inviscid analysis of transonic and low Reynolds number airfoils, AIAA journal, 25, 1347–1355, 1987.

Drela, M. and Youngren, H.: Xfoil subsonic airfoil development system, Open source software available at http://web. mit. edu/drela/Public/web/xfoil, 2008.

Fischer, A., Flamm, A., Jost, E., Lutz, T., and Krämer, E.: Numerical investigation of a model wind turbine, in: Contributions to the 21st STAB Symposium Braunschweig, Germany 2016, Notes on Numerical Fluid Mechanics and Multidisciplinary Design, STAB, Springer, accepted for publication, 2016.

Huang, X., Vey, S., Meinke, M., Schroeder, W., Pechlivanoglou, G., Nayeri, C., and Paschereit, C. O.: Numerical and Experimental Investigation of Wind Turbine Wakes, in: 45th AIAA Fluid Dynamics Conference, p. 2310, https://doi.org/10.2514/6.2015-2310, 2015.

Jameson, A.: Time dependent calculations using multigrid, with applications to unsteady flows past airfoils and wings, AIAA paper, 1596, 1991, 1991.

Jameson, A., Schmidt, W., Turkel, E., et al.: Numerical solutions of the Euler equations by finite volume methods using Runge-Kutta time-stepping schemes, AIAA paper, 1259, 1981, 1981.

Johansen, J. and Sørensen, N. N.: Aerofoil characteristics from 3D CFD rotor computations, Wind Energy, 7, 283–294, https://doi.org/10.1002/we.127, 2004.

Jost, E.: personal communication, Institute of Aerodynamics and Gas Dynamics, 2017.

Jost, E., Fischer, A., Lutz, T., and Krämer, E.: An investigation of unsteady 3D effects on trailing edge flaps, in: Journal of Physics: Conference Series, vol. 753, p. 022009, IOP Publishing, 2016.

Klein, A., Zabel, S., Lutz, T., and Krämer, E.: About the influence of wind tunnel walls, tower and nozzle on the performance of a model wind turbine, in: High Performance Computing in Science and Engineering´ 17, Springer, accepted for publication, 2017.

Klein, L.: personal communication, Institute of Aerodynamics and Gas Dynamics, 2017.

Klein, L., Lutz, T., and Krämer, E.: CFD analysis of a 2-bladed multi-megawatt turbine, in: 10th PhD Seminar on Wind Energy in Europe, pp. 47–50, 28-31 October 2014, Orléans, France, 2014.

Kowarsch, U., Öhrle, C., Keßler, M., and Krämer, E.: Aeroacoustic Simulation of a complete H145 Helicopter in descent flight, Journal of the American Helicopter Society, 61, 1–13, https://doi.org/10.4050/JAHS.61.042001, 2016.

Kroll, N., Rossow, C., Becker, K., and Thiele, F.: The MEGAFLOW project, Aerosp. Sci. Technol., 4, 223–237, https://doi.org/10.1016/S1270-9638(00)00131-0, 2000.

Marten, D., Pechlivanoglou, G., Nayeri, C., and Paschereit, C.: Integration of a WT Blade Design tool in XFOIL/XFLR5, in: 10th German Wind Energy Conference (DEWEK 2010), Bremen, Germany, Nov, pp. 17–18, 2010.

Marten, D., Lennie, M., Pechlivanoglou, G., Nayeri, C., and Paschereit, C.: Integration of an Unsteady Nonlinear Lifting Line Free Vortex Wake Algorithm in a Wind Turbine Design Framework, in: EWEA Annual Meeting, Paris, Nov, pp. 17–20, 2015.

Marten, D., Lennie, M., Pechlivanoglou, G., Nayeri, C. N., and Paschereit, C. O.: Implementation, optimization, and validation of a nonlinear lifting line-free vortex wake module within the wind turbine simulation code qblade, Journal of Engineering for Gas Turbines and Power, 138, 072 601, https://doi.org/10.1115/1.4031872, 2016.

Meister, K.: Numerische Untersuchung zum aerodynamischen und aeroelastischen Verhalten einer Windenergieanlage bei turbulenter atmosphärischer Zuströmung, Shaker Verlag, 2015.

Montgomerie, B.: Methods for Root Effects, Tip Effects and Extending the Angle of Attack Range to+-180°, with Application to Aerodynamics for Blades on Wind Turbines and Propellers, Swedish Defence Research Agency, 2004.

Nayeri, C. N., Vey, S., Marten, D., Pechlivanoglou, G., Paschereit, C. O., Huang, X., Meinke, M., Schöder, W., Kampers, G., Hölling, M., Peinke, J., Fischer, A., Lutz, T., Krämer, E., Cordes, U., Hufnagel, K., Schiffmann, K., Spiegelberg, H., and Tropea, C.: Collaborative Research on Wind Turbine Load Control under Realistic Tubulent Inflow Conditions, 12th German Wind Energy Conference (DEWEK 2015), Bremen, Germany, May, 2015.

Pechlivanoglou, G., Fischer, J., Eisele, O., Vey, S., Nayeri, C. N., and Paschereit, C. O.: DEVELOPMENT OF A MEDIUM SCALE RESEARCH HAWT FOR INFLOW AND AERODYNAMIC RESEARCH IN THE TU BERLIN WIND TUNNEL, 12th German Wind Energy Conference (DEWEK 2015), Bremen, Germany, May, 2015.

Sayed, M., Lutz, T., and Krämer, E.: Aerodynamic investigation of flow over a multi-megawatt slender bladed horizontal-axis wind turbine, Renewable Energies Offshore, 2015.

Schepers, J. and Snel, H.: Model experiments in controlled conditions, ECN Report: ECN-E-07-042, 2007.

Schepers, J. G.: Engineering models in wind energy aerodynamics: Development, implementation and analysis using dedicated aerodynamic measurements, Aerospace Engineering. Delft University of Technology, https://doi.org/10.4233/uuid:92123c07-cc12-4945-973f-103bd744ec87, 2012.

Schulz, C., Letzgus, P., Lutz, T., and Krämer, E.: CFD study on the impact of yawed inflow on loads, power and near wake of a generic wind turbine, Wind Energy, 20, 253–268, https://doi.org/10.1002/we.2004, 2017.

Schümann, H., Pierella, F., and Sætran, L.: Experimental investigation of wind turbine wakes in the wind tunnel, Energy Procedia, 35, 285–296, https://doi.org/10.1016/j.egypro.2013.07.181, 2013.

Simms, D., Schreck, S., Hand, M., and Fingersh, L.: NREL unsteady aerodynamics experiment in the NASA-Ames wind tunnel: a comparison of predictions to measurements, Tech. rep., National Renewable Energy Lab., Golden, CO (US), 2001.

Van Garrel, A.: Development of a wind turbine aerodynamics simulation module, Technical Report, ECN, 2003.

Vey, S., Marten, D., Pechlivanoglou, G., Nayeri, C., and Paschereit, C. O.: Experimental and Numerical Investigations of a Small Research Wind Turbine, in: 33rd AIAA Applied Aerodynamics Conference, June, pp. 1–9, American Institute of Aeronautics and Astronautics, Reston, Virginia, https://doi.org/10.2514/6.2015-3392, 2015.

Wendler, J., Marten, D., Pechlivanoglou, G., Nayeri, C., and Paschereit, C.: Implementation and Validation of an Unsteady Aerodynamics Model for Horizontal and Vertical Axis Wind Turbines Within the Simulation Tool QBlade, GT2016-57184, Accepted for: ASME Turbo Expo, 2016.